Geophysical Research Letters

RESEARCH LETTER
10.1029/2023GL103689

Key Points:

- A new application using tomographic imaging of electrostatic auroral arcs with ALIS estimates the magnetospheric generator state
- The generator of the arc observed by ALIS appears to be a plasma interface at the contact between trough and plasma sheet-like plasmas
- The arc's longitudinal changes are linked to a tailward increase of electron temperature and dawnward indentation of the generator interface

Supporting Information:

Supporting Information may be found in the online version of this article.

Correspondence to:

M. Echim,
marius.echim@aeronomie.be

Citation:

Echim, M., Lamy, H., Simon-Wedlund, C., De Keyser, J., & Cessateur, G. (2023). Probing the magnetospheric generator of quiet electrostatic auroral arcs from ground based optical observations and magnetosphere-ionosphere coupling modeling. *Geophysical Research Letters*, *50*, e2023GL103689. https://doi.org/10.1029/2023GL103689

Received 3 APR 2023
Accepted 15 NOV 2023

Author Contributions:

Conceptualization: M. Echim
Formal analysis: M. Echim, G. Cessateur
Funding acquisition: M. Echim, H. Lamy, J. De Keyser
Investigation: C. Simon-Wedlund, J. De Keyser, G. Cessateur
Methodology: M. Echim, H. Lamy, C. Simon-Wedlund, J. De Keyser, G. Cessateur
Project Administration: M. Echim, H. Lamy, J. De Keyser
Resources: M. Echim, H. Lamy, J. De Keyser

Probing the Magnetospheric Generator of Quiet Electrostatic Auroral Arcs From Ground Based Optical Observations and Magnetosphere-ionosphere Coupling Modeling

M. Echim[1,2,3], H. Lamy[1,3], C. Simon-Wedlund[4], J. De Keyser[1,3], and G. Cessateur[1,3]

[1]The Royal Belgian Institute for Space Aeronomy, Brussels, Belgium, [2]Institute of Space Science, Măgurele, Romania, [3]Solar-Terrestrial Center of Excellence, Brussels, Belgium, [4]Space Research Institute of the Austrian Academy of Sciences, Graz, Austria

Abstract Observations of a quiet electrostatic auroral arc by the ALIS network on 5 March 2008 are used to infer a two-dimensional map of the flux of precipitating energy. Among a family of numerical solutions of a stationary magnetosphere—ionosphere coupling model in which the origin of the arc is a magnetospheric generator interface, we find which generator interface properties best fit the observed precipitating energy flux. The procedure finds that the plasma populations in the generator are colder and more rarefied on one side of the interface and warmer and denser on the other side, similar to a transition between plasma trough and plasma sheet plasmas. The increase of the arc's brightness, the decrease of its thickness and its slight spatial undulation may be driven by an increase of plasma sheet electron temperature in the tailward direction, tangential to the interface, and a local spatial indentation in the dawn-ward direction.

Plain Language Summary Optical observations of aurora provide information about the local electromagnetic and plasma conditions in the ionosphere where the impact of energetic electrons produces auroral light emissions. The electrons gain energy through acceleration by static or dynamic electric fields along their path from the magnetospheric source to the upper ionized atmosphere where they collide with various atomic species, like oxygen and nitrogen, which emit light at various wavelengths. In this paper we use optical observations of a steady electrostatic auroral arc to identify the conditions in the magnetospheric source that best fit these observations in the context of an electrostatic auroral acceleration model. This way, optical auroral observations from the ground are used as a remote sensing tool to probe the magnetospheric source of the arc.

1. Introduction

The Auroral Large Imaging System (ALIS) is a network of observatories in Northern Scandinavia targeting the auroral ionosphere from different vantage points, equipped with narrow-band interference filters centered on the N2+ 1NG blue line at 4278 Å and the atomic O green and red lines at 5577 Å and 6300 Å. Tomography-like techniques (Gustavsson, 1998, Gustavsson, 2000) allow to reconstruct the 3-D volume emission rate (VER) at each observed wavelength. The temporal resolution is 5–20 s, depending on the filter sequence (Simon Wedlund et al., 2013 and references therein). Since the 4278 Å blue line is produced by impact of precipitating electrons on the thermosphere only, the 3-D 'blue' VER is inverted to compute a 2-D map of the electron precipitation flux with a fast parametrized kinetic transport model of the ionosphere (Sergienko & Ivanov, 1993). Simon Wedlund et al. (2013) used this two-step reconstruction method to retrieve the 2-D precipitating flux for a steady auroral arc observed on 5 March 2008.

The coupling of a steady electrostatic auroral arc with its magnetospheric source can be described by a kinetic model of magnetospheric interface generators (MIG) (Borovsky et al., 2019; Echim et al., 2007; Roth et al., 1993). In this model, finite gyroradius effects generate an electric field at the interface between two magnetospheric plasmas with different properties. Behaving like a battery, the generator is coupled to the ionospheric load (ionospheric energy dissipation, including the auroral emission) by magnetic field lines along which electrons and protons move in the mirroring field geometry. Analytical expressions for the parallel current density carried by these species ($J_{\parallel}$) as a function of the field aligned potential drop, $\Delta\Phi = \Phi_i - \Phi_m$, between the magnetospheric generator potential (Φ_m) and the ionospheric potential (Φ_i) are given by current-voltage relationships

Software: M. Echim, C. Simon-Wedlund, G. Cessateur
Validation: M. Echim, H. Lamy, C. Simon-Wedlund, J. De Keyser, G. Cessateur
Visualization: M. Echim, C. Simon-Wedlund, G. Cessateur
Writing – original draft: M. Echim
Writing – review & editing: M. Echim, H. Lamy, C. Simon-Wedlund, J. De Keyser, G. Cessateur

proposed by, for example, Knight (1973), Lemaire and Scherer (1971, 1973), Fridman and Lemaire (1980), and Pierrard (1996).

The current in the auroral circuit is conserved. This allows the computation of the ionospheric electrostatic potential, Φ_i, when Φ_m is known (e.g., L. Lyons, 1981; Lyons et al., 1979). We assume Φ_m is provided by the MIG model. Thus, the M-I coupling model gives $\Delta\Phi$ and all the auroral variables depending on it (De Keyser & Echim, 2013; De Keyser et al., 2010; Echim et al., 2007, 2008). This model was applied in past studies to find a solution for the "direct" problem: estimate the properties of an auroral arc for given magnetospheric interface generator properties (e.g., Echim et al., 2009; Johnson & Wing, 2015; Wing & Johnson, 2015).

In this study we use the quasi-stationary M-I coupling model and optical observations from ALIS to solve the "inverse" problem, that is, to estimate the magnetospheric plasma state at the source of an electrostatic arc whose properties are known. For a family of magnetospheric source parameters, the M-I coupling model computes the MIG configurations and the corresponding auroral arc solutions (AAS) in the form of one-dimensional profiles across the arc. This produces profiles of the flux of precipitating energy (ε), field-aligned current density ($J_{\parallel}$), ionospheric electrostatic potential (Φ_i), and field-aligned potential drop ($\Delta\Phi$). Echim et al. (2019) proposed to search for which family member the AAS matches the observations of the arc best. Each member of the AAS family, called *set_ARC*, is compared quantitatively with experimental observations through a least-squares minimization procedure. The resulting set of magnetospheric source parameters is considered to provide the best estimate for the generator state. Here, we combine this methodology with tomography-like reconstruction of optical auroral emission (Gustavsson, 1998; Simon Wedlund et al., 2013) to provide the data against which to evaluate each AAS. For slightly spatially undulating auroral arcs such as the one considered here, we can even obtain a two-dimensional reconstruction of the magnetospheric interface generator. The method and the observations are briefly presented in Section 2. The magnetospheric plasma state and the link with the auroral properties observed by ALIS is discussed in Section 3. A summary and perspective are included at the end.

2. Methodology, Tomographic Data, Ensemble of M-I Coupling Model Solutions

Figure 1 illustrates the results of the tomography-like reconstruction of auroral images (Simon Wedlund et al., 2013) recorded by ALIS on 5 March 2008. The two successive inversions (tomography-like 3-D reconstruction and inversion of the blue VER) make use of the Multiplicative Algebraic Reconstruction Technique (MART) and provide a 2-D map of ε, the flux of precipitating energy. The steady electrostatic arc is observed on the dusk side (19 LT). Figure 1 also shows 1-D slices of the map of ε at three different longitudes, $y = -48$ km, $y = -18$ km, $y = +18$ from Skibotn.

We adapt the procedure put forward by Echim et al. (2019) for the particular auroral observables provided by ALIS. We define a dimensionless defect norm that measures how well the model quantities $\varepsilon^{\text{model}}$ fits the observations ε^{obs}:

$$S^{(\varepsilon)}_{\text{NORM}} = \sum_{i=1}^{N} \frac{\sqrt{|(\varepsilon_i{}^{\text{model}})^2 - (\varepsilon_i{}^{\text{ALIS}})^2|}}{|\varepsilon_i{}^{\text{ALIS}}|}, \tag{1}$$

where $\varepsilon^{\text{ALIS}}$ is the precipitating energy flux obtained from the tomography-like analysis and $\varepsilon^{\text{model}}$ is given by the M-I coupling model. Both are provided as discrete time series consisting of N samples.

The reconstructed flux of precipitating energy, $\varepsilon^{\text{ALIS}}$, is provided as function of latitude and longitude, see Figure 1. However, the M-I coupling model provides the 1-D flux of precipitating energy as a function of the direction normal to the arc. To compute $S^{(\varepsilon)}_{\text{NORM}}$ one needs to extract 1-D slices from $\varepsilon^{\text{ALIS}}$; since the arc is at essentially constant latitude, such slices are obtained for fixed values y of the longitude: $\epsilon^{\text{ALIS}}_y(x_i) = \varepsilon^{\text{ALIS}}(x_i, \text{y})$. We consider three cuts: for $y = -48$ km (relative to Skibotn), $y = -18$ km, and $y = +18$ km. The variables $\epsilon^{\text{ALIS}}_y(x_i)$ and $\epsilon^{\text{model}}(x_i)$ are resampled such that both have an equal number of N samples.

For 30 different configurations of MIG we compute 30 AAS solutions which form our set of electrostatic auroral arc models, *set_ARC*. A discussion on the MIG configurations is given in the next section. The defect norm, $S^{(\epsilon)}_{\text{NORM}}$, defined by Equation 1, is then computed for each profile of the model precipitating energy flux, ϵ^{model}. The procedure thus provides 30 values for $S^{(\epsilon)}_{\text{NORM}}$, one for each model AAS. The model that minimizes $S^{(\epsilon)}_{\text{NORM}}$

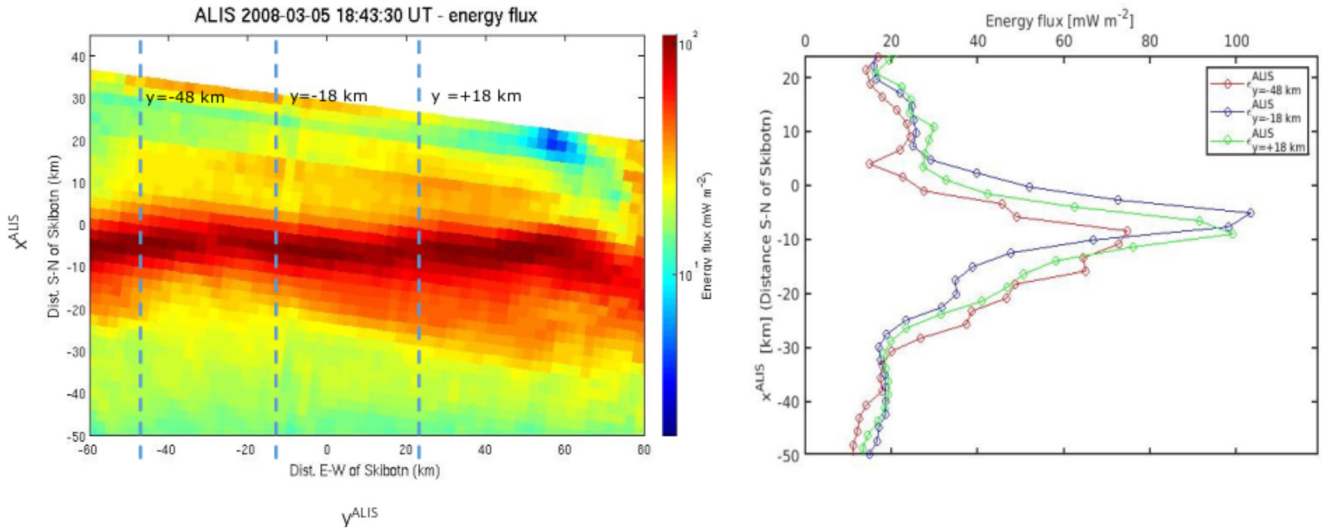

Figure 1. (left) The 2-D flux of precipitating energy reconstructed from ALIS observations of an electrostatic auroral arc on 05/03/2008. (right) 1-D slices extracted from the 2-D map at three different longitudes: $y = -48$ km eastward from Skibotn (red, $\epsilon^{\mathrm{ALIS}}_{y=-48}$), $y = -18$ km eastward from Skibotn (blue, $\epsilon^{\mathrm{ALIS}}_{y=-18}$), and $y = +18$ km westward from Skibotn (green, $\epsilon^{\mathrm{ALIS}}_{y=+18}$).

represents the solution closest to the ALIS observations, $\epsilon^{\mathrm{model}}_{\mathrm{sol}}$. The corresponding magnetospheric interface configuration, $\mathrm{MIG}_{\mathrm{sol}}$, is then our estimation for the plasma state at the magnetospheric source of the arc, as discussed in the next section.

We apply this procedure for each of the three ALIS profiles illustrated in the right panel of Figure 1. The results are shown in Figure 2, where the three panels illustrate the $S^{(\epsilon)}_{\mathrm{NORM}}$ values computed for the three experimental profiles, $\epsilon^{\mathrm{ALIS}}_{y=-48}$, $\epsilon^{\mathrm{ALIS}}_{y=-18}$, $\epsilon^{\mathrm{ALIS}}_{y=+18}$. The experimental data and model solution in Equation 1 need to be aligned peak

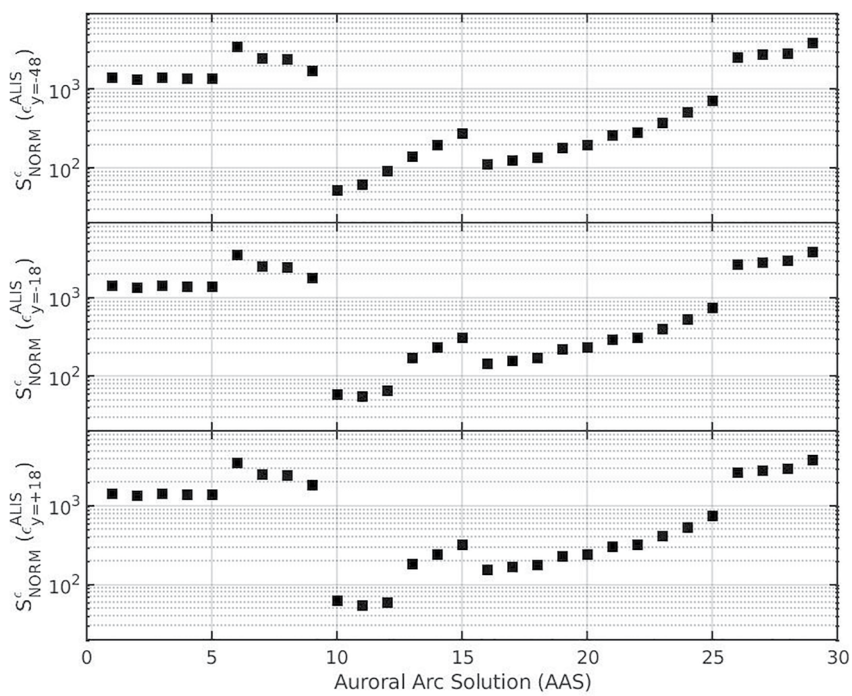

Figure 2. Defect measure $S^{(\epsilon)}_{\mathrm{NORM}}$, defined by Equation 1 computed for three profiles of the flux of precipitating energy, $\epsilon^{\mathrm{ALIS}}_{y=-48}(x_i)$, $\epsilon^{\mathrm{ALIS}}_{y=-18}(x_i)$, $\epsilon^{\mathrm{ALIS}}_{y=+18}(x_i)$, and 30 solutions of $\epsilon^{\mathrm{model}}$ included in *set_ARC*. The three experimental profiles are extracted from the 2-D map $\epsilon^{\mathrm{ALIS}}_{y}(x_i, y_i)$ shown in Figure 1 for the three azimuthal positions $y = -48$ km, $y = -18$ km and $y = +18$ km.

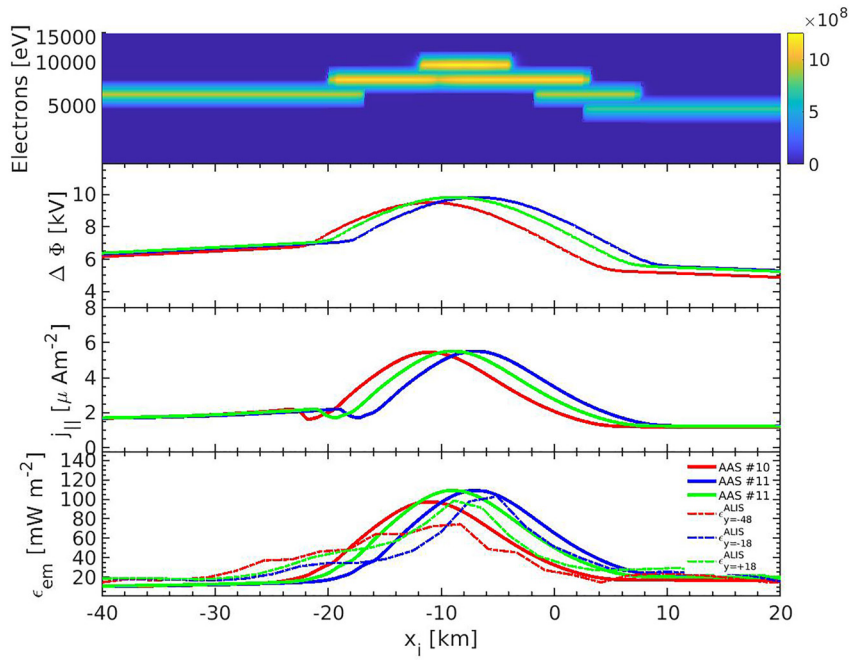

Figure 3. Illustration of Auroral Arc solution AAS#10, two instances of Auroral Arc solution AAS#11 and the three 1-D profiles provided by ALIS tomographic reconstruction and inversion of blue line (Simon Wedlund et al., 2013); the two instances of model AAS#11 are displaced one with respect to the other by $\Delta x = 7$ km such that their center of the transition coincides. The panels show: (a) the Arc Model flux of precipitating energy at 260 km altitude for a Maxwellian population of electrons injected at generator altitude (4.3 R_E) in the field-aligned potential drop provided by the model; (b) the Arc Model field-aligned potential drop; (c) the Arc Model field-aligned current density; (d) the flux of precipitating energy carried by the down going electrons. Continuous line profiles show the Arc Models AAS#10 and AAS#11; dashed lines profiles show the 1-D cuts through the 2-D reconstructed map, $\epsilon^{\mathrm{ALIS}}_{y=-48}$, $\epsilon^{\mathrm{ALIS}}_{y=-18}$, $\epsilon^{\mathrm{ALIS}}_{y=+18}$.

to peak, to avoid obtaining large values of $S^{(\epsilon)}_{\mathrm{NORM}}$ for profiles very similar in shape and scale but misaligned in space. Thus, before computing $S^{(\epsilon)}_{\mathrm{NORM}}$ the experimental profiles are displaced by a distance Δx in the direction normal to the arc such that the maximum of $\epsilon^{\mathrm{ALIS}}_{y}(x_i)$ is at $x_i = 0$; this condition is achieved by default for all model solutions in *set_ARC*.

We found that the reconstructed ALIS profile $\epsilon^{\mathrm{ALIS}}_{y=-48}$, is best approximated by the arc model AAS#10, see Figure 2. The reconstructed ALIS profiles $\epsilon^{\mathrm{ALIS}}_{y=-18}$ and $\epsilon^{\mathrm{ALIS}}_{y=+18}$ are best estimated by the arc model AAS#11 (middle and bottom panels in Figure 2). Note however that the best fit of $\epsilon^{\mathrm{ALIS}}_{y=+18}$ is obtained when the Model AAS#11 is displaced Northward by a distance $\Delta x = 10$ km. AAS#11 provides a best fit for the experimental profile $\epsilon^{\mathrm{ALIS}}_{y=-18}$ for $\Delta x = 0$. Figure 3 illustrates a selection of auroral properties from auroral arc models AAS#10 and AAS#11; the bottom panel shows ε computed by the model as well as the experimental 1-D profiles extracted from the ALIS map. Model solutions AAS#10 and AAS#11 reflect the experimental data very well in terms of amplitude and spatial scale of the peak value. In the next section we discuss the properties of the magnetospheric generator at the origin of arc model solutions AAS#10 and AAS#11.

3. Properties of the Magnetospheric Generator at the Origin of the Arc Observed by ALIS Network

The different magnetospheric generator configurations considered at the origin of the 30 arc models included in *set_ARC* have one common feature: they describe the tangential contact between a colder and less dense plasma, similar to plasma trough material, with a warmer and denser one, typical of the plasma sheet. A small bulk velocity tangential to the interface (and perpendicular to the magnetic field) is considered at both sides. The 30 MIG models are obtained from Vlasov-Maxwell equilibrium solutions (Roth et al., 1996) for various asymptotic values of the electron temperature and density at the warmer, plasma-sheet-like (right) side of the interface. In addition, we also varied the magnetic field intensity at the center of the magnetospheric interface, which is equivalent to

changing the altitude of the generator, assuming the magnetic intensity changes with the altitude as in a dipole model. The three parameters mentioned above control the thickness of the magnetospheric plasma interface and the intensity of the polarization electric field across the interface. The latter has an impact on the accelerating potential, $\Delta\Phi$, obtained between the generator and the auroral arc and hence on the flux of precipitating energy. The M-I coupling model also assumes a cylindrical geometry in altitude, such that the scales perpendicular to the magnetic field changes (are compressed) in altitude proportional to $\sqrt{\frac{B_m}{B_i}}$ where B_m and B_i are the magnetic field intensity at generator's altitude z_m, and auroral arc's altitude z_i, respectively (Echim et al., 2007).

The MIG models #1 to #5, which are at the origin of arc models AAS#1 to AAS#5, are obtained by increasing the asymptotic electron density on the plasma-sheet-like side of the interface, from 0.15 to 0.9 cm^{-3}, with a minimum step $\Delta n = 0.05$ cm^{-3}. All the other asymptotic parameters are kept unmodified. MIG models #6 to #15 are derived by varying the asymptotic electron temperature on the plasma-sheet-like side: an increase from 100 to 9,000 eV (models #6 to #13) and a decrease from 8,000 eV to 3,000 eV (models #14 to #15), with a minimal step $\Delta T_e = 100$ eV. MIG models #16 to #30 are derived by changing the magnetic field intensity in the center of the interface from $B_{m1} = 460$ nT to $B_{m2} = 380$ nT, with a minimal step $\Delta Bm = 15$ nT. The range assumed for magnetic intensity corresponds to a range of generator altitudes between $z_{m1} = 4.26\ R_E$ and $z_{m2} = 4.54\ R_E$, respectively. The "resolution" of our MIG parametric description is defined by the minimal steps assumed for the variable parameters specified above.

In Figure 4 we illustrate the three MIG models at the origin of the auroral arc models presented in Figure 3. The MIG models provide a pseudo two-dimensional reconstruction of the magnetospheric generator structure, assuming that the 2-D image of the generator can be derived from a series of 1-D slices. Such an approach is justified for a planar arc, that is, the arc is at most slightly undulating. Figure 4 shows the variation across the magnetospheric interface of three variables, plasma density, electron temperature and electric potential; note that the Vlasov-Maxwell solution provides the entire set of plasma moments.

The results shown in Figure 4 suggest that the generator of the auroral arc observed by ALIS is a plasma interface between cold and warmer plasmas. At the colder side the plasma density is 0.21 cm^{-3}, the asymptotic temperature of electrons and protons is 75 and 500 eV, respectively; the perpendicular bulk velocity of electrons and protons ions is 0.5 and 15 km/s, respectively. At the warmer side, the plasma density is equal to 0.3 cm^{-3} the electron temperature is 6,000 eV or larger; such temperatures are typical of the plasma sheet (e.g., Thomsen et al., 1996). The density shows a peak in the center of the interface which is due to a population trapped inside the interface. Interestingly, in order to fit the scale of the transition a small contribution of cold trapped up-flowing oxygen ions was added (De Keyser et al., 2017).

5th of March 2008 was a geomagnetically relatively calm day. D_{ST} and AE indices had low to moderate values and no substorms were ongoing at the moment of ALIS observations of the quasi-quiet electrostatic auroral arc. The OVATION-PRIME statistical model of the auroral oval, based on DMSP observations (available from NASA-CCMC, included in the Supporting Information S1) suggests the arc observed by ALIS is located at the equatorial edge of the auroral oval. A mapping of the arc in the equatorial magnetospheric tail can also be inferred from specific arc/precipitation boundaries, like, for example, the isotropic precipitation boundary from in-situ spectra of high energetic electrons and ions (Sergeev et al., 1983, 1993, 2020; Yahnin et al., 1997, see also Feldstein & Galperin, 1985, 1999). Data from the polar spacecraft NOAA 17 confirm the location of the arc at the equatorward boundary of the oval. Thus, the mapping and location of the arc suggest the generator low temperature population corresponds most likely to the plasma trough. As a summary, we find the generator at the origin of the electrostatic auroral arc observed by ALIS is an interface formed between plasma sheet and plasma trough, in the magnetospheric dusk sector, at an altitude equal roughly to $z_m = 4.2\ R_E$.

To estimate the relative orientation of the X^{GEN} and Y^{GEN} directions in Figure 4, and of the 2D reconstruction of the generator interface, we mapped the entire 2D map of the arc reconstructed from ALIS data (shown in Figure 1) with the Tsyganenko2001 magnetic field model (available from NASA CCMC). The mapping, presented in the Supporting Information S1, indicates the Y^{GEN} direction (tangential to the interface) in Figure 4 is roughly aligned with the GSM Ox axis, and X^{GEN} direction (normal to the interface) is roughly aligned with the GSM Oy direction. In other words, the magnetospheric interface is roughly aligned with the Sun-Earth direction. Thus, the increase of the electron temperature along Y^{GEN} direction at the warmer side of the interface shown in Figure 4 corresponds to a gradient in the tailward direction. We also note that the center of the magnetospheric

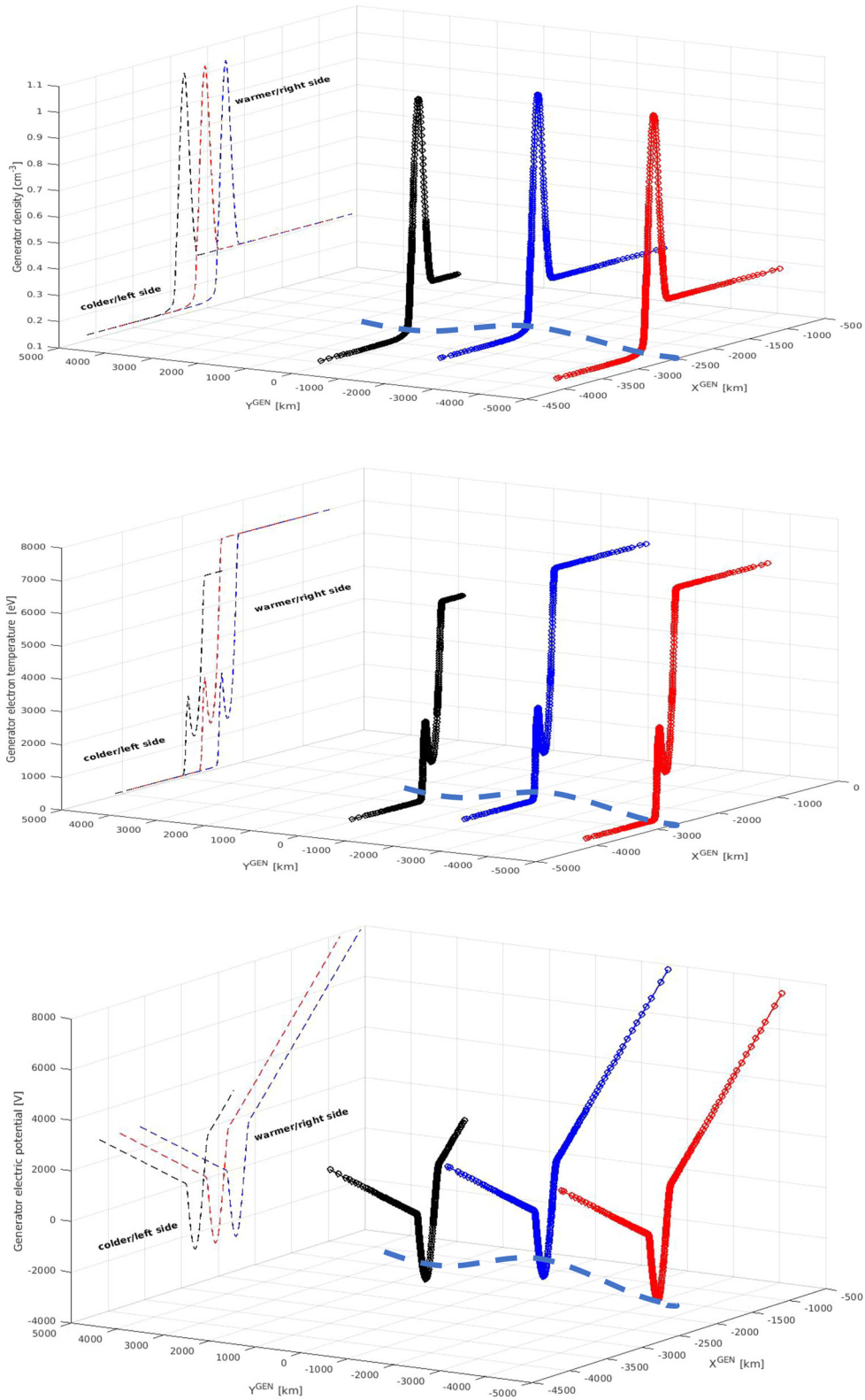

Figure 4.

interface at $Y^{GEN} = -2{,}000$ km (the blue profile in Figure 4) is displaced with respect to the centers of the other two 1D slices by a distance $\Delta X^{GEN} = 500$ km in the dawnward direction.

We searched for spacecraft data in the sector pointed out by the mapping discussed above. THEMIS D crossed around 21:00 UT the magnetospheric dusk sector in the targeted region and measured electron and ion temperatures and densities equal to $T_{ePS} = 2{,}000$ eV, $T_{iPS} = 3{,}000$ eV, $n_{ePS} = 0.8$ cm^{-3}, $n_{iPS} = 0.9$ cm^{-3}, suggesting a plasma sheet population. Nevertheless, around 19:00 UT, THEMIS-D intersects the interface between trough plasma and plasma sheet, at earlier local times than the mapped position of the arc. The plasma sheet temperatures and densities measured by THEMIS-D at 19:00 UT of the order of 1000 eV for electrons and 2,000 eV for ions. The colder electron and ion temperatures and densities provided by THEMIS-D at 19:00 UT are equal to $T_{eL} = 100$ eV, $T_i = 200$ eV, $n_{eL} = 0.3$ cm^{-3}, $n_{iL} = 1$ cm^{-3}. THEMIS-D data are included in the Supporting Information S1. In order to better understand the global magnetospheric context, we also performed global MHD simulations with LFM code on NASA-CCMC tailored for the interplanetary conditions derived from OMNI database for 5th of March 2008. The mapping of the auroral arc observed by ALIS along Tsyganenko2001 model field lines of the simulated magnetosphere points to an interface between the plasma sheet and low density and cold plasma (shown in the Supporting Information S1). All these findings converge toward a scenario where a plasma interface formed at the edge of the plasma sheet is at the origin of the arc observed by ALIS. OVATION-PRIME and LFM numerical simulations results as well as THEMIS-D data are included as a Supporting Information S1.

From the results shown in Figures 1, 3, and 4 the following scenario is derived. ALIS data reveal a quiet electrostatic arc whose thickness increases slightly with longitude; also the arc's luminosity is relatively more intense at its Eastward side. The center of the arc is slightly indented toward North. These longitudinal variations can be linked to slow changes along the magnetospheric generator interface formed between plasma sheet and plasma trough populations. The dimming and thinning of the arc correspond to an increase of the plasma-sheet-like electron temperature, from 6 to 7 keV, in the tailward direction, tangential to the interface. The 2D reconstruction of the magnetospheric interface reveals a local indentation over 500 km in the dawnward direction which can be linked to the arc's displacement in the Northward direction.

4. Summary and Perspectives

We have introduced a new tool to examine steady electrostatic auroral arcs. We use a magnetosphere-ionosphere coupling model to calculate the auroral signature of a family of magnetospheric generator models derived from Vlasov equilibrium solutions calculated for tangential plasma interfaces. We provide a two-dimensional reconstruction of the magnetospheric generator plasma state based on the two-dimensional map of precipitating energy flux derived from optical observations by the ALIS network of auroral observatories on 5th Marc 2008. The procedure searches which arc model fits best the observations. Below we summarize our findings on the magnetospheric origin of the arc observed by ALIS on 5th of March 2008:

- "*Where*": the magnetospheric interface generator is found at the contact between plasma sheet-like plasma and trough plasma at roughly 4 R_E above the arc;
- "*When*": during relatively geomagnetically quiet times, when electrostatic conditions apply;
- "*Why*": the generator interface at the origin of the arc is formed as a tangential kinetic equilibrium between two plasmas with different properties, that sustains a V-shaped electrostatic potential that drives the auroral current system, with field-aligned currents closing through the topside ionosphere;
- "*How*": this current system leads to the formation of a parallel potential difference accelerating electrons downward into the auroral ionosphere; the relative increase of the arc's brightness in the azimuthal direction may be induced by a tailward increase of the plasma sheet electron temperature. The small displacement of the auroral arc in the Northward direction (approximately 10 km, as suggested by optical data) may be explained by a local indentation (over roughly 500 km) of the magnetospheric plasma generator interface.

A limitation of our approach is that it assumes electrostatic auroral acceleration and thus disregards rapid temporal variations of the generator. It also assumes that the two-dimensional profile of the magnetospheric interface

Figure 4. Description of MIG at the origin of the quiet electrostatic arc observed by ALIS on 5 March 2008 at 18:43:30 UT. Upper panel shows three 1-D cuts through the generator density; middle panel shows three 1-D cuts through the generator electron temperature; lower panels show the three 1-D cuts through the generator electrostatic potential. Negative Y^{GEN} axis points roughly in the tailward direction, X^{GEN} axis points toward dawn (according to Tsyganenko mapping of the arc, see the Supporting Information S1). The dashed blue line suggests the position of the interface's center interpolated from the positions of the centers of the three 1D cuts; the blue profile is indented with respect to the other two by roughly $\Delta X^{GEN} = 500$ km in the dawnward direction.

generator can be built from a collection of one-dimensional slices. A true two-dimensional model of the generator may help to overcome this limitation; such a model could describe more complex features like, for example, bead-like structures linked to the nonlinear evolution of magnetospheric sheared flow layers (Johnson et al., 2021). However, this is beyond reach of the 1-D kinetic equilibrium model that is used here to compute the generator structure.

Nevertheless, when the arc does have a slow/adiabatic time variation one can also attempt a reconstruction of the evolution of the magnetospheric generator following the technique demonstrated above if the time dependence results from a sequence of different quasi-stationary states. Other types of magnetospheric generators and acceleration mechanisms, adequate for more dynamic arcs, can be included in the procedure to increase its capabilities to reconstruct the magnetospheric plasma state from optical observations of auroral arcs.

Data Availability Statement

ALIS data recorded on 5 March 2008 are freely available from https://alis.irf.se/stdnames/2008/03/05/. All the figures included in this paper, the data leading to these figures, the MIG models and the set_ARC family of auroral arcs models included in set_ARC, as well as the computer scripts (in matlab) allowing to reproduce the figures are available from M. Echim (2023).

Acknowledgments
The authors acknowledge support from the Belgian BRAIN-BE project BR/175/A2/MOMA. MME, HL, JDK, GC acknowledge support from the Belgian Solar Terrestrial Center of Excellence (STCE). MME acknowledges support from the Belgian PRODEX project Cluster and BRAIN-BE2 project B2/223/P1/PLATINUM. The authors also acknowledge NASA-CCMC for providing the support for running models and simulations like the empirical statistical auroral oval model OVATION-PRIME, and the global MHD numerical simulations of the Earth's magnetosphere with BATS-RUS and LFM codes. Marius Echim thanks Mr. Umar Sayed, the librarian of the Royal Belgian Institute for Space Aeronomy, for his constant and efficient collaboration. CSW acknowledges support from the Austrian Science Fund (FWF) project FWF project P35954-N.

References

Borovsky, J. E., Birn, J., Echim, M. M., Fujita, S., Lysak, R. L., Knudsen, D. J., et al. (2019). Quiescent discrete auroral arcs: A review of magnetospheric generator mechanisms. *Space Science Reviews*, *216*, 1. https://doi.org/10.1007/s11214-019-0619-5

De Keyser, J., & Echim, M. (2013). Electric potential differences across auroral generator interfaces. *Annales Geophysicae*, *31*(2), 251–261. https://doi.org/10.5194/angeo-31-251-2013

De Keyser, J., Maes, L., Maggiolo, R., & Haaland, S. (2017). Magnetopause thickness at the dawn and dusk flanks. In S. Haaland, A. Runov, & C. Forsyth (Eds.), *Dawn-dusk asymmetries in planetary plasma environments, geophysical monograph 230* (1st ed.). American Geophysical Union. John Wiley & Sons, Inc.

De Keyser, J., Maggiolo, R., & Echim, M. (2010). Monopolar and bipolar auroral electric fields and their effects. *Annales Geophysicae*, *28*(11), 2027–2046. https://doi.org/10.5194/angeo-28-2027-2010

Echim, M. (2023). Data and software to estimate the properties of the magnetospheric generator from ALIS observations of an auroral arc on 05/03/2008 [Dataset]. Royal Belgian Institute for Space Aeronomy (BIRA-IASB). https://doi.org/10.18758/71021082

Echim, M. M., Lamy, H., De Keyser, J., Maggiolo, R., Gunell, H., & Simon Wedlund, C. L. (2019). A method to estimate the physical properties of magnetospheric generators from observations of quiet discrete auroral arcs. *Journal of Geophysical Research: Space Physics*, *124*(12), 10283–10293. https://doi.org/10.1029/2019JA026969

Echim, M. M., Maggiolo, R., Roth, M., & De Keyser, J. (2009). A magnetospheric generator driving ion and electron acceleration and electric currents in a discrete auroral arc observed by Cluster and DMSP. *Geophysical Research Letters*, *36*(12), L12111. CiteID. https://doi.org/10.1029/2009GL038343456

Echim, M. M., Roth, M., & De Keyser, J. (2007). Sheared magnetospheric plasma flows and discrete 460 auroral arcs: A quasi-static coupling model. *Annales Geophysicae*, *25*(Issue 1), 317–330. https://doi.org/10.5194/angeo-25-317-2007

Echim, M. M., Roth, M., & De Keyser, J. (2008). Ionospheric feedback effects on the quasi-stationary coupling between LLBL and postnoon/evening discrete auroral arcs. *Annales Geophysicae*, *26*(4), 913–928. https://doi.org/10.5194/angeo-26-913-2008

Feldstein, Y. I., & Galperin, Y. I. (1985). The auroral luminosity structure in the high-latitude upper atmosphere: Its dynamics and relationship to the large-scale structure of the Earth's magnetosphere. *Reviews of Geophysics*, *23*(3), 217–275. https://doi.org/10.1029/rg023i003p00217

Feldstein, Y. I., & Galperin, Y. I. (1999). Comment on 'Magnetospheric source region of discrete auroras inferred from their relationship with isotropy boundaries of energetic particles' by A. G. Yahnin et al. *Annales Geophysicae*, *17*, 37–41. https://doi.org/10.1007/s00585-999-0037-1

Fridman, M., & Lemaire, J. (1980). Relationship between auroral electron fluxes and field-aligned electric potential differences. *Journal of Geophysical Research*, *85*(A2), 664–670. https://doi.org/10.1029/ja085ia02p00664

Gustavsson, B. (1998). Tomographic inversion for ALIS noise and resolution. *Journal of Geophysical Research*, *103*(A11), 26621–26632. https://doi.org/10.1029/98JA00678

Gustavsson, B. (2000). Three dimensional imaging of aurora and airglow, Institutet för rymdfysik (IRF). *Scientific Reports*, *267*.

Johnson, J. R., & Wing, S. (2015). The dependence of the strength and thickness of field-aligned currents on solar wind and ionospheric parameters. *Journal of Geophysical Research: Space Physics*, *120*(5), 3987–4008. https://doi.org/10.1002/2014JA020312

Johnson, J. R., Wing, S., Delamere, P., Petrinec, S., & Kavosi, S. (2021). Field-aligned currents in auroral vortices. *Journal of Geophysical Research: Space Physics*, *126*(2), e2020JA028583. https://doi.org/10.1029/2020JA028583

Knight, S. (1973). Parallel electric fields. *Planetary and Space Science*, *21*(5), 741–750. https://doi.org/10.1016/0032-0633(73)90093-7

Lemaire, J., & Scherer, M. (1971). Simple model for an ion-exosphere in an open magnetic field. *Physics of Fluids*, *14*(8), 1683–1694. https://doi.org/10.1063/1.1693664

Lemaire, J., & Scherer, M. (1973). Plasma sheet particle precipitation: A kinetic model. *Planetary and Space Science*, *21*(2), 281–289. https://doi.org/10.1016/0032-0633(73)90012-3

Lyons, L. (1981). Discrete aurora as the direct result of an inferred high altitude generating potential distribution. *Journal of Geophysical Research*, *86*(1–8), 1–8. https://doi.org/10.1029/ja086ia01p00001

Lyons, L. R., Evans, D. S., & Lundin, R. (1979). An observed relation between magnetic field aligned electric fields and downward electron energy fluxes in the vicinity of auroral forms. *Journal of Geophysical Research*, *84*(A2), 457–461. https://doi.org/10.1029/ja084ia02p00457

Pierrard, V. (1996). New model of magnetospheric current-voltage relationship. *Journal of Geophysical Research*, *101*(A2), 2669–2676. https://doi.org/10.1029/95ja00476

Roth, M., De Keyser, J., & Kuznetsova, M. M. (1996). Vlasov theory of the equilibrium structure of tangential discontinuities in space plasmas. *Space Science Reviews*, *76*(3–4), 251–317. https://doi.org/10.1007/BF00197842

Roth, M., Evans, D., & Lemaire, J. (1993). Theoretical structure of a magnetospheric plasma boundary: Application to the formation of discrete auroral arcs. *Journal of Geophysical Research*, *98*(A7), 11411–11423. https://doi.org/10.1029/93ja00156

Sergeev, V., Bondareva, T., Gilles, D., & Donovan, E. (2020). On the source region and orientations of nightside auroral arcs. *Journal of Atmospheric and Solar-Terrestrial Physics*, *204*, 105288. https://doi.org/10.1016/j.jastp.2020.105288

Sergeev, V. A., Malkov, M., & Mursula, K. (1993). Testing the isotropic boundary algorithm method to evaluate the magnetic field configuration in the tail. *Journal of Geophysical Research*, *98*(A5), 7609–7620. https://doi.org/10.1029/92ja02587

Sergeev, V. A., Sazhina, E. M., Tsyganenko, N. A., Lundblad, J. Å., & Søraas, F. (1983). Pitch-angle scattering of energetic protons in the magnetotail current sheet as the dominant source of their isotropic precipitation into the nightside ionosphere. *Planetary and Space Science*, *31*(10), 1147–1155. https://doi.org/10.1016/0032-0633(83)90103-4

Sergienko, T. I., & Ivanov, V. E. (1993). A new approach to calculate the excitation of atmospheric gases by auroral electron impact. *Annales Geophysicae*, *11*, 717–727.

Simon Wedlund, C., Lamy, H., Gustavsson, B., Sergienko, T., & Brändström, U. (2013). Estimating energy spectra of electron precipitation above auroral arcs from ground-based observations with radar and optics. *Journal of Geophysical Research: Space Physics*, *118*(6), 3672–3691. https://doi.org/10.1002/jgra.50347

Thomsen, M. F., Borovsky, J. E., McComas, D. J., & Moldwin, M. B. (1996). Observations of the Earth's plasma sheet at Geosynchronous Orbit. *AIP Conference Proceedings*, *383*, 25–31. https://doi.org/10.1063/1.51535

Wing, S., & Johnson, J. R. (2015). Theory and observations of upward field-aligned currents at the magnetopause boundary layer. *Geophysical Research Letters*, *42*(21), 9149–9155. https://doi.org/10.1002/2015GL065464

Yahnin, A. G., Sergeev, V. A., Gvozdevsky, B. B., & Vennerstrøm, S. (1997). Magnetospheric source region of discrete auroras inferred from their relationship with isotropy boundaries of energetic particles. *Annales Geophysicae*, *15*(8), 943–958. https://doi.org/10.1007/s00585-997-0943-z